

# Characterization of sequential exocytosis in a human neuroendocrine cell line using evanescent wave microscopy and “virtual trajectory” analysis

Viet Samuel Tran · Sébastien Huet · Isabelle Fanget ·  
Sophie Cribier · Jean-Pierre Henry · Erdem Karatekin

Received: 22 December 2006 / Revised: 16 March 2007 / Accepted: 20 March 2007 / Published online: 18 April 2007  
© EBSA 2007

**Abstract** Secretion of hormones and other bioactive substances is a fundamental process for virtually all multicellular organisms. Using total internal reflection fluorescence microscopy (TIRFM), we have studied the calcium-triggered exocytosis of single, fluorescently labeled large, dense core vesicles in the human neuroendocrine BON cell line. Three types of exocytotic events were observed: (1) simple fusions (disappearance of a fluorescent spot by rapid diffusion of the dye released to the extracellular space), (2) “orphan” fusions for which only rapid dye diffusion, but not the parent vesicle, could be detected, and (3) events with incomplete or multi-step disappearance of a fluorescent spot. Although all three types were reported previously, only the first case is clearly understood. Here, thanks to a combination of two-color imaging, variable angle TIRFM, and novel statistical analyses, we show that the latter two types of events are generated by the same basic mechanism, namely shape retention of fused vesicle ghosts which become targets for

sequential fusions with deeper lying vesicles. Overall, ~25% of all exocytotic events occur via sequential fusion. Secondary vesicles, located 200–300 nm away from the cell membrane are as fusion ready as primary vesicles located very near the cell membrane. These findings call for a fundamental shift in current models of regulated secretion in endocrine cells. Previously, sequential fusion had been studied mainly using two-photon imaging. To the best of our knowledge, this work constitutes the first quantitative report on sequential fusion using TIRFM, despite its long running and widespread use in studies of secretory mechanisms.

## Introduction

Regulated exocytosis involves the  $\text{Ca}^{2+}$ -triggered fusion of secretory vesicles with the plasma membrane, allowing vesicle contents to be released to the cell exterior. Fusion may be followed by the complete release and collapse of the vesicular membrane into the plasma membrane (full fusion), or alternatively, the fusion pore may open and then close again after release of a fraction of the vesicle contents (“kiss-and-run” fusion, An and Zenisek 2004). More recently, a type of fusion named sequential exocytosis has been described using visualization of the influx of an extracellular dye through the open fusion pore using two-photon imaging (Nemoto et al. 2001; Kishimoto et al. 2005, 2006; Pickett and Edwardson 2006). In this case, an initial primary fusion event at the plasma membrane results in a stably fused vesicle, which then becomes a target for secondary fusion events with deeper-lying vesicles. Sequential exocytosis seems to occur commonly, at least for the fusion of large, dense-core vesicles (LDCVs, also

**Electronic supplementary material** The online version of this article (doi:10.1007/s00249-007-0161-3) contains supplementary material, which is available to authorized users.

V. S. Tran · S. Huet · I. Fanget · J.-P. Henry ·  
E. Karatekin (✉)  
Institut de Biologie Physico-Chimique, CNRS, UPR 1929,  
Université Paris 7 Denis Diderot, Paris, France  
e-mail: erdem@ibpc.fr

S. Cribier  
CNRS, UMR 7099, Université Pierre et Marie Curie-Paris 6,  
Paris, France

*Present Address:*  
S. Huet  
Department of Gene Expression and Cell Biology/Biophysics,  
EMBL, Meyerhofstrasse 1, 69117 Heidelberg, Germany

called secretory granules), in pancreatic acinar cells (almost all events, Nemoto et al. 2001), parotid and nasal acinar cells (Pickett and Edwardson 2006), pancreatic  $\beta$ -cells (~5% of all events, Takahashi et al. 2002), neuroendocrine chromaffin (>70%, Kishimoto et al. 2006) and PC12 cells (>75%, Kishimoto et al. 2005).

In this article, we present evidence for the retention of vesicular shapes following exocytosis and sequential fusion occurring to a significant extent in endocrine BON cells, using total internal reflection fluorescence microscopy (TIRFM), also called evanescent wave microscopy (Steyer and Almers 2001; Axelrod 2003). The BON cell line is derived from a human metastatic carcinoid tumor from the pancreas. Carcinoid tumors are neuroendocrine tumors derived from enterochromaffin cells and constitute a morphologically and physiologically diverse group, synthesizing chromogranin A and a variety of bioactive substances, including serotonin, histamine, prostaglandins, as well as neurotensin and other regulatory peptides. In the normally functioning gut, the coordinated release of intestinal peptides by enterochromaffin cells in response to extracellular mediators is essential for the regulation of intestinal digestion, secretion and motility. Hypersecretion of these amines and peptides from carcinoid tumors may cause a devastating range of effects together known as the carcinoid syndrome with characteristic symptoms such as cutaneous flushing, abdominal cramping, diarrhea, bronchospasm, and tricuspid valve thickening (Jackson et al. 2006; Evers et al. 1994).

The BON cell line established and characterized in the laboratory of J. C. Thompson (Evers et al. 1994) display morphological and biochemical characteristics consistent with the enterochromaffin cell phenotype, including the presence of numerous LDCVs and the expression and secretion of chromogranin A, serotonin, pancreastatin, neurotensin and other peptides. Such properties are very close to those of the specialized N cell of the small intestine (Li et al. 2005b). In addition, BON cells display proliferation and invasiveness characteristic of carcinoid tumor cells (Jackson et al. 2006). Thus, the BON cell line has been increasingly used as a model in studies of mechanisms underlying stimulated gut peptide secretion from normal, specialized enterochromaffin cells of the gastrointestinal tract (Li et al. 2005a, b, 2004), and of neuroendocrine carcinoid tumor hormone secretion, growth and invasion (Evers et al. 1991, 1994; Kim et al. 2001; Jackson et al. 2006; Mergler 2003; Mergler et al. 2005, 2003). More importantly, it currently represents one of the only carcinoid cell lines available. Beside its importance in understanding secretion mechanisms operating in the gut and in carcinoid tumors, these cells are easily cultured and transfected compared to chromaffin or other primary cell cultures, and thus constitute a convenient model for

studying calcium-triggered exocytosis of secretory granules in general.

We have previously used TIRFM to study dynamics of single secretory vesicles in BON cells (Huet et al. 2006). Here, also using TIRFM, we demonstrate that an important fraction (~25%) of all exocytotic events in these cells occurs through sequential fusion. Although previously suggested hitherto, to the best of our knowledge, sequential fusion had never been quantified using TIRFM. This is paradoxical, since TIRFM is arguably the most commonly utilized method for studying single vesicle dynamics and exocytosis in live cells [for reviews, see, e.g., An and Zenisek 2004; Steyer and Almers 2001; Axelrod 2003; Schneckenburger 2005]. We suggest this has been mostly due to ambiguities in interpretation of some TIRFM data, and present ways to overcome them thanks to a combination of variable angle TIRFM, two-color live imaging, and novel statistical analyses. The frequent occurrence of sequential fusion suggests a fundamental shift in current models of regulated secretion by endocrine cells.

## Materials and methods

### Cell culture and vesicle labeling

Cells were cultured and labeled as described in Huet et al. (2006). The human carcinoid BON cell line was kindly provided by C. M. Townsend (University of Texas Medical Branch, Galveston, TX, USA). Lumens of LDCVs were labeled using the chimera neuropeptide Y-green fluorescent protein (NPY-GFP), which is the fusion between the human proneuropeptide Y and the enhanced green fluorescent protein (Lang et al. 1997). Expression of NPY-GFP was induced by transfection with a plasmid, kindly provided by W. Almers (Oregon Health Sciences University, Portland, OR, USA), as described (Huet et al. 2006). Either the original cell line ("wild type", WT) or a subclone named N13, generated in our laboratory (Fang et al., unpublished data) were used in the TIRFM experiments. Following transfection, cells were plated onto uncoated glass-bottom dishes (P50G-1.5-14-F, MatTek Cultureware, Ashland, MA, USA). Observations were performed at 31–33°C, between 48 and 72 h after plating, in Locke solution (5.6 mM Glucose, 3.6 mM HCO<sub>3</sub><sup>-</sup>, 159.6 mM Cl<sup>-</sup>, 157.6 mM Na<sup>+</sup>, 5.6 mM K<sup>+</sup>, 5 mM HEPES-NaOH, 2.5 mM CaCl<sub>2</sub>, 1.2 mM MgCl<sub>2</sub>).

### TIRFM observations and data analysis

The setup and calibration are described in detail in Huet et al. (2006). Briefly, an upright microscope (BX50WI,

Olympus, Tokyo) was adapted to TIRFM by use of a hemisphere, allowing convenient variation of the incidence angle and hence the evanescence depth,  $\delta$ . An evanescent wave was generated using the 488 nm or 514 nm line of an argon laser (177-G02, Spectra Physics, Newport, Irvine, CA, USA) radially entering a BK7 glass hemisphere from its curved side. The beam totally reflected off the planar face of the hemisphere which was optically coupled to a glass-bottom culture dish using immersion oil (518°C, Carl Zeiss MicroImaging, Inc., Oberkochen, Germany). During stream acquisition, laser power was attenuated to  $\sim 1$  mW and illumination was restricted to image acquisition by a shutter coupled to the camera in order to minimize photobleaching. Cells were observed through a water immersion objective (Olympus LUMPlanFL/IR  $60 \times /0.9$  numerical aperture), and frames were captured with a charge-coupled device camera (CoolSnap HQ, Photometrics, Roper Scientific, Tucson, AZ, USA) after choosing a region of interest typically encompassing a single cell. Under these conditions, one pixel corresponded to 107.5 nm. Frames were acquired for 60–120 s at 2–40 Hz using Metamorph software (Universal Imaging, Molecular Devices Corp., Downingtown, PA, USA).

Most vesicles appeared as diffraction-limited fluorescent spots, since their sizes were similar to those obtained with 200 nm diameter fluorescent beads. Single exocytic events were detected manually, using time derivatives of image sequences of the form  $\{f'_{j-n}\} = \{f_j - f_{j-n}\}_{j=n, n+1, n+2, \dots}$ , where  $\{f_j\}$  is the original sequence of images,  $\{f'_{j-n}\}$  is the time derivative image sequence,  $n$  is the “time step” used in the derivative calculation and  $j$  is an index for frame numbers in a sequence. The choice of  $n$  depends on the acquisition rate and the speed with which a fluorescent spot disappears from view during acquisition; the best value of  $n$  being that which optimizes visual detection of exocytosis. For a typical acquisition rate of 10 Hz and fusion time  $\sim 100$  ms,  $n = 2$ – $3$  were found to be optimal by trial and error. The position and the frame number of each detected exocytosis event was marked.

Spots for which residual fluorescence remained after an exocytosis event were tracked, provided the signal-to-noise ratio (S/N) permitted this. First, 2D ( $xy$ ) fluorescent spot trajectories in the imaging plane were obtained from stacks of images by single particle tracking (SPT) using the Metamorph software. We did SPT one spot at a time. The position of a given spot ( $xy$  coordinates) on every frame was detected as the centroid of the corresponding pixels (Cheezum et al. 2001). To minimize positioning error, it was important to exclude as much of the image background as possible from the centroid calculation. This was achieved by setting a threshold brightness. Pixel values

below the threshold were taken to be zero whereas those above remained unchanged. Employing “dynamic thresholding”, i.e., by adjusting the threshold along the trajectory, it was possible to keep tracking a spot, even after a sudden and important loss of intensity, as occurs upon exocytosis.

“Virtual trajectories” of fluorescent spots along the  $z$ -axis (perpendicular to the glass-solution interface) were calculated as follows. We first evaluated the fluorescence intensity of a spot in a given frame by plotting radially averaged pixel values as a function of distance from the center of the spot. The intensity of a spot was defined as the area under a Gaussian fit to this profile, with the tail of the Gaussian set to zero amplitude. This amounts to subtracting the local background; upon complete disappearance of a spot, the calculated intensity drops to zero (i.e., to the local background level). Evanescent field profiles at various incidence angles were calibrated experimentally, as described in Huet et al. (2006). The measured profiles were well-fitted by simple exponential decays of the form  $I = I_o e^{-z/\delta}$ , where  $z$  is a distance along the  $z$ -axis. This relation was inverted to calculate the “trajectory” of a fluorescent spot in the  $z$  direction:  $z(t) = -\delta \ln(I(t)/I_o)$ . Fluorescence intensity traces were rescaled such that  $I = I_o$  just before a fusion event (see Fig. 6a). We averaged 5–10 points just preceding an exocytosis event to define  $I_o$ . The “virtual jump size”,  $\Delta z$ , corresponding to a fusion event was calculated from the  $z(t)$  traces, typically averaging 5–10 points preceding and following a fusion event.  $z$ -positions of a fluorescent spot displaying residual fluorescence upon exocytosis *do not* refer to physical displacements of a vesicle (see Fig. 4). Hence, we refer to them as “virtual trajectories”. Analysis of such trajectories can be used to distinguish between different mechanisms that could generate residual fluorescence following a fusion event, since each distinct mechanism leads to distinct jump-size statistics (see Sect. [Residual fluorescence after an exocytosis, possible mechanisms generating it, and how to distinguish among them using the “virtual trajectory” analysis](#)).

For two-color experiments (Figs. 2, 3), excitation (488 and 514 nm lines of the laser) and emission (515–550 band-pass and  $> 515$  high-pass) were alternated synchronously. Data were acquired at 2.5 Hz per channel. For these experiments only, the fluorescence intensity of a spot was defined as the mean pixel value of a small region of interest encompassing the spot ( $8 \times 8$  pixels for Fig. 2 and  $6 \times 8$  pixels for Fig. 3). The mean pixel value of a nearby region without distinct features was taken as the background intensity and subtracted from the original signal. The intensity traces in Figs. 2 and 3 are shifted vertically for clarity.

## Cell stimulation

### *Stimulation by UV-uncaging of calcium*

Cells were incubated at 37°C for 60 min in Locke buffer with 30  $\mu\text{M}$  o-nitrophenyl-EGTA-acetoxymethyl ester (NP-EGTA-AM, Invitrogen, Carlsbad, CA, USA) followed by 60 min incubation in the culture medium. Under the TIRF microscope, 6 or 8 brief pulses of UV light were generated every 6 or 10 s using a Xenon arc flash lamp (Rapp Optoelectronic, Hamburg, Germany) coupled to the epifluorescence port of the microscope using a liquid light guide. In these experiments,  $[\text{Ca}^{2+}]_i$  rises almost instantaneously upon photolysis of the NP-EGTA with a UV pulse, then decreases roughly exponentially in 3–6 s (Karatekin et al. in preparation).

### *Stimulation using digitonin permeabilization in the presence of calcium*

In order to clamp the calcium concentration to a known and well-controlled value, we placed cells in a potassium glutamate medium containing 30  $\mu\text{M}$  free calcium (150 mM potassium glutamate, 20 mM PIPES, 2 mM HEDTA, 2 mM EGTA, 2 mM ATP, 0.3 mM GTP, 4.1 mM  $\text{MgCl}_2$ , 2.5 mM  $\text{CaCl}_2$  and 0.3% BSA, pH adjusted to 7.0 using KOH. The free  $[\text{Ca}^{2+}]$  and  $[\text{Mg}^{2+}]$  are calculated to be 30  $\mu\text{M}$  and 1 mM, respectively, using the programs MaxChelator (<http://www.stanford.edu/~cpatton/maxc.html>, Patton et al. 2004), and Calcv22 (Fohr et al. 1993) just before TIRFM observations. Single cells were permeabilized by a 20 s superfusion with the same buffer supplemented by 20  $\mu\text{M}$  digitonin (Tran et al. 2004). A glass or quartz micropipette (opening diameter 10–100  $\mu\text{m}$ ), connected to a perfusion system (model BPS-4, ALA Scientific Instruments, Inc., Westbury, NY, USA) was used to superfuse a single cell, while a second, larger micropipette, placed at the other side of the cell, was used to aspirate the stimulation solution. This helped avoid stimulating other cells in the dish, so that up to ~10 cells could be stimulated per dish one after another. Image acquisition typically started just before the superfusion of the cell under observation.

### *Stimulation using $\text{Ba}^{2+}$*

For some of the two-color experiments in the presence of tetramethylrhodamine-dextran (TMRhod-dextran), cells were stimulated using a 20 s superfusion with 3.7 mM  $\text{Ba}^{2+}$  (as for the data in Fig. 2), in a medium composed of 5.6 mM glucose, 157.8 mM  $\text{Cl}^-$ , 157.8 mM  $\text{Na}^+$ , 5.5 mM  $\text{K}^+$ , 15 mM HEPES (pH 7.4), and 3.7 mM  $\text{Ba}^{2+}$ . For the

rest of the two-color experiments we used UV uncaging of calcium (as for the data in Fig. 3).

Residual fluorescence following exocytosis and “orphan” fusions (Sect. [Vesicle ghosts lingering at the cell membrane after exocytosis and “orphan” fusion events are both part of a sequential fusion mechanism](#)) were observed with all types of stimulation, with apparently similar characteristics.

### Two-color experiments using tetramethylrhodamine-dextran (TMRhod-dextran)

For experiments probing shape retention after exocytosis, 50  $\mu\text{M}$  tetramethylrhodamine labeled 3-kDa dextran (TMRhod-dextran, Invitrogen, Carlsbad, CA, USA) was added to the usual observation buffer. The evanescence depth was set to 200 nm in order to reduce signals from TMRhod-dextran relative to NPY-GFP labeled, deeper lying vesicles. In the red TMRhod-dextran channel, cell footprints appeared negatively stained. This staining was not homogeneous and depended on the thickness of the irregular space between the cell-membrane and the glass surface. In principle, washing away the dextran should allow distinguishing between shape retention with a dilated fusion pore versus transient fusion (Fig. 4b vs. c). Unfortunately, in practice, washing was too slow and usually perturbed the cell’s adhesion to allow clear observations.

## Results

### Visualization of different types of single exocytotic events

Using TIRFM, we visualized LDCVs in endocrine BON cells by labeling secretory vesicle contents by a neuropeptide-Y-green fluorescent protein construct (see “[Materials and methods](#)”). In this technique, a laser beam totally reflected off the glass coverslip-aqueous solution interface generates an evanescent wave which decays exponentially as a function of distance from the interface, with a characteristic decay length of the order of 100 nm. Thus, only those labeled vesicles which are close to the cell membrane adhering to the coverslip are visualized. Such vesicles appear as diffraction-limited fluorescent spots in the evanescent field, since typical vesicle sizes are 200–300 nm.

Cells were stimulated for secretion using either ultraviolet uncaging of a “caged calcium” compound previously loaded into the cytosol, or permeabilization via digitonin in the presence of 30  $\mu\text{M}$   $\text{Ca}^{2+}$ . Single exocytotic events were visualized by the sudden disappearance of a fluorescent spot, accompanied by rapid diffusion of dye

which had been expelled into the thin space between the cell membrane and the coverslip. Spontaneous exocytosis events in the absence of stimulation were extremely rare, while upon raising the intracellular concentration,  $[Ca^{2+}]_i$ , we typically obtained a robust secretory response including complete disappearance of all vesicles that were visible in the evanescent field in a few cells. This confirms that LDCV exocytosis in BON cells is calcium-triggered (Kim et al. 2001; Mergler et al. 2003; Tran et al. 2004). Three types of single exocytotic events were detected, as follows:

1. In most cases (70%, 1,207 of all 1,721 exocytosis events) the original signal disappeared completely within 100–200 ms, consistent with a vesicle releasing all its contents, as shown in Fig. 1a.
2. In many other cases, a “puff” of fluorescence appeared suddenly, without a detectable prior signal (which would correspond to a parent vesicle), and disappeared by diffusing away rapidly, also within 100–200 ms (Fig. 1b). Since the parent vesicles could not be identified for this type of fusion event, we refer to it as “orphan fusion”.
3. In yet another type of fusion event, after an exocytosis occurred at a fluorescent spot, careful inspection

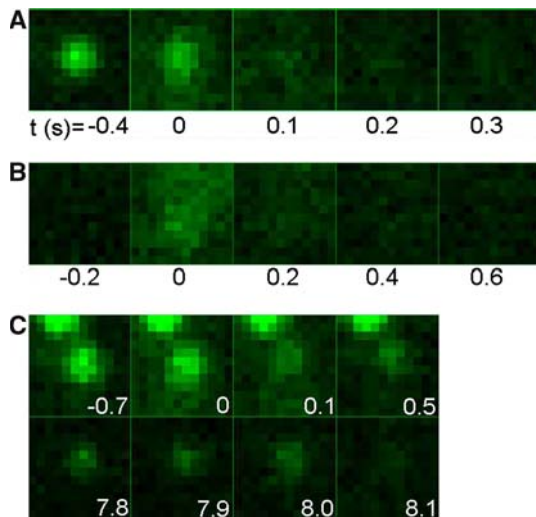


**Fig. 1** Different types of exocytosis observed using TIRFM. **a** A “normal” exocytosis event. A fluorescent spot, visible for at least several frames rapidly disappears as soluble vesicular fluorescent labels, released to the extracellular space, diffuse away. **b** An “orphan” fusion. This type displays the same post-fusion characteristics as normal fusion, yet the parent vesicle somehow escapes detection. **c** Incomplete/multi-step disappearance of a spot. In this example, the fluorescent spot in the middle disappeared in two steps. The first step marks  $t = 0$  s and is accompanied by a sudden spread of dye (frames marked 0 and 0.1), characteristic of single exocytotic events. Some fluorescence remained thereafter, at the same spot (0.5–7.9 s). A second fusion occurred at 8.0 s (see Movie 1 in Supplementary material). Each frame corresponds to a  $1.3 \times 1.3 \mu\text{m}^2$  box

revealed that a faint fluorescent signal remained at the same position as the original one (Fig. 1c). Some of these residual signals disappeared later in what appeared to be single exocytotic events characterized by rapid disappearance accompanied by dye diffusion.

The first type of exocytosis described above has been thoroughly studied in many cell types [reviewed in, e.g., Steyer et al. (1997); An and Zenisek (2004)], including BON cells [Tran et al. (2004), and Karatekin et al., in preparation]. The last two types of event have also been reported previously for chromaffin and PC-12 cells (Ma et al. 2004; Taraska et al. 2003; Allersma et al. 2004, 2006). However, mechanisms generating them are controversial and far from being clear. Understanding their origin is the main objective of this work.

In the next section, we will present our results on orphan fusions and show that a large subset of these arise from a sequential fusion mechanism for which retention of vesicular shape after exocytosis is a prerequisite. In Sect. [Residual fluorescence after an exocytosis, possible mechanisms generating it, and how to distinguish among them using the “virtual trajectory” analysis](#), we will describe how to distinguish among the different possible mechanisms that can generate residual fluorescence after an exocytosis event thanks to a novel approach we call “virtual trajectory analysis”. In Sects. [“Adjacent vesicle fusion”](#) and [“Transient versus sequential fusion”](#) we will apply our virtual trajectory analysis to exocytosis events which left behind residual signals. We will finish with a discussion in Sect. [Discussion](#).

Vesicle ghosts lingering at the cell membrane after exocytosis and “orphan” fusion events are both part of a sequential fusion mechanism

In sequential fusion, the  $\Omega$ -shaped profile of a secretory vesicle recently fused with the cell membrane (a vesicle “ghost”) must be conserved long enough till a second vesicle queued up behind the first one fuses with it. Hence, survival of vesicular ghost shapes is a prerequisite for sequential fusion to occur.

Retention of vesicular shape after fusion has been demonstrated in numerous other cell types using two-photon and confocal microscopies (Pickett and Edwardson 2006; Kishimoto et al. 2006; Sokac and Bement 2006), scanning ion conductance microscopy (Shin and Gillis 2006), and TIRFM (Taraska et al. 2003; Allersma et al. 2004). It is thought that the collapse of the vesicular ghosts into the cellular membrane is prevented by rapid F-actin coating of the freshly fused vesicles (Pickett and Edwardson 2006; Nemoto et al. 2004; Sokac and Bement 2006), a

process named “kiss-and-coat” exocytosis (Sokac and Bement 2006). In cells in which sequential exocytosis occurs to a significant extent, ghost shapes were found to survive for at least a few seconds, long enough to allow fusion of the vesicles queued-up behind (Nemoto et al. 2001; Kishimoto et al. 2006, 2005). In the pancreatic acini where sequential exocytosis occurs probably with the highest frequency encountered to date, zymogen granules freshly fused with the plasma membrane maintain their  $\Omega$ -shaped profiles for an average of 220 s (Nemoto et al. 2001).

It is essential to note that the “kiss-and-coat” mechanism described above is quite distinct from the so called “kiss-and-run” events observed in the fusion of synaptic vesicles in neurons (Aravanis et al. 2003). The latter refers to short-lived, transient fusion events in which typically a pore of a few nanometers in diameter connects the vesicle to the cell’s exterior for only  $<1$  s (Aravanis et al. 2003; Sokac and Bement 2006; Lindau and Alvarez de Toledo 2003). In kiss-and-coat exocytosis, on the other hand, “pores” connecting vesicle ghosts to the cell’s exterior can be as large as the diameter of a vesicle and can survive up to minutes (reviewed in Sokac and Bement 2006). In addition, the fate of a vesicle ghost in kiss-and-coat exocytosis is more colorful: it can eventually end up collapsing slowly into the cell-membrane, become a target for sequential fusion with a deeper lying secondary vesicle (Nemoto et al. 2001; Kishimoto et al. 2006, 2005), and finally, there are indications that it may be taken up back into the cell (i.e., endocytosed) en bloc, a process named “granule cavity recapture”, or “cavcapture” (Taraska et al. 2003, see also Sokac and Bement 2006).

We have studied the conservation of the shapes of freshly fused vesicles in BON cells using a tetramethylrhodamine labeled 3-kDa dextran added as an extracellular soluble label. The dextran filled the thin region between the glass coverslip and the adherent cells. Upon exocytosis, if a vesicle ghost’s shape is retained, the red dextran should fill up the newly created cavity in the cell membrane. This process should be observed as the disappearance of a green spot, marking soluble vesicular labels prior to fusion, simultaneously with the appearance of a red signal in the same spot. We have observed many such events, as shown in Fig. 2. The red fluorescent dots, hence the fused vesicle ghosts, had lifetimes of 5–15 s.

In fact, transient kiss-and-run type of fusion events with pores large enough to allow passage of the 3-kD dextran (hydrodynamic radius  $\approx 4$  nm, Takahashi et al. 2002) might also lead to similar observations. On rare occasions, however, we observed events such as in Fig. 3 which cannot be explained by transient fusion. Here, the apparently complete disappearance of a vesicle’s contents at  $t = 0$  s is accompanied by the simultaneous appearance of the red

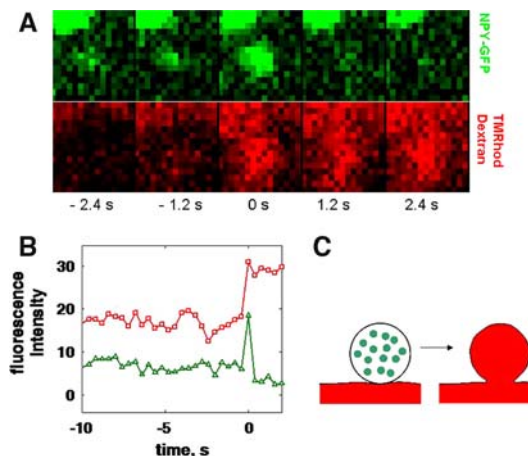


**Fig. 2** Shape conservation after fusion. **a** *Top panel* shows the green signal from NPY-GFP, labeling lumens of vesicles. *Bottom panel* shows signals from TMRhod-dextran filling the thin gap between the cell and the coverslip. The sequence of images from which this montage is extracted is shown in Movie 3 (Supplementary material). **b** Fluorescence intensity as a function of time for the NPY-GFP (green triangles) and TMRhod-dextran (red squares) channels. **c** Schematic description of the interpretation of the observations in **a** and **b**

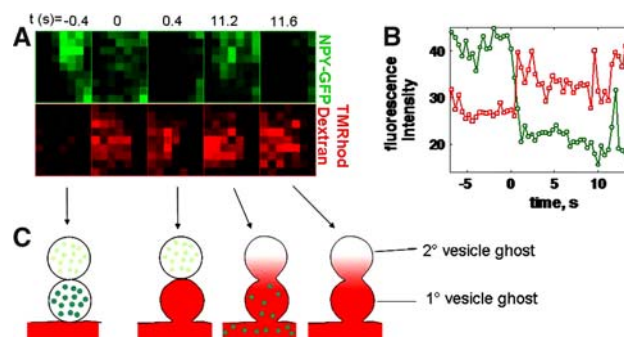


**Fig. 3** Shape conservation after exocytosis and “orphan” fusion. **a** *Top panel* shows the green signal from NPY-GFP, marking the lumens of the vesicles. *Bottom panel* shows signals from the TMRhod-dextran filling the thin gap between the cell and the coverslip. An “orphan” fusion event is detected in the green channel at 11.2 s, concomitant with a second sudden increase of the red channel signal. **b** Fluorescence intensity as a function of time for the NPY-GFP (green circles) and TMRhod-dextran (red squares) channels. **c** Schematic description of the interpretation of the observations in **a** and **b**

dextran signal, filling the vesicular space. After 11.2 s, succeeding this first fusion, an orphan fusion event was detected in the green channel, concomitant with a stepwise increase in the red signal. Most likely, the orphan event was due to a secondary vesicle, which was just outside the evanescent field, fusing with the ghost of the primary vesicle which had undergone a fusion event earlier, at time  $t = 0$  (Fig. 3c). Upon fusion of the secondary vesicle, its soluble luminal labels are released into, and must diffuse

**Table 1** Orphan fusions and fusions for which residual fluorescence was observed at different evanescence depths,  $\delta$ 

	$\delta = 100$ nm		$\delta = 150$ nm		Total
	Number	%	Number	%	
All detected fusion events	1,196		525		1,721
Residual fluorescence	112	9.4	101	19.2	213
Orphans within footprint	160	13.4	36	6.9	196
Combined	272	22.7	137	26.1	23.8%

through, the space connecting it to the exterior space, thereby entering the evanescent field and becoming visible briefly before diffusing away.

In faster, single-color acquisition experiments we observed many orphan events. Some of these occurred at borders of cellular footprints, suggesting that the invisible parent vesicles were located on the lateral cell membrane, outside the evanescent field (105 of all 1,721 events). However, we also observed many orphan fusions well within cellular footprints (196/1,721 events). These could be due to sequential events, with parent vesicles located in the second, third, etc., layers deep in the cytosol. If this is the case, then a higher proportion of orphan events should be detected in experiments employing thinner evanescence depths,  $\delta$ , since it would be more difficult to detect secondary, tertiary parent vesicles. We have indeed observed a considerably higher proportion of orphan events (well within footprints) at  $\delta = 100$  nm (160/1,196 events, or 13.4%) than at  $\delta = 150$  nm (36/525 events, or 6.9%), as shown in Table 1.

Residual fluorescence after an exocytosis, possible mechanisms generating it, and how to distinguish among them using the “virtual trajectory” analysis

Careful inspection revealed that a faint fluorescent spot remained after many exocytosis events, apparently at the same position as the original signal, as shown in Fig. 1c (213/1,721 events, or 12%, 55 cells). In some cases, the remaining spot disappeared, after a delay  $\Delta t$ , giving off a fluorescent “puff”, characteristic of exocytosis ( $n = 71$  events, 22 cells). Rarely, a yet weaker fluorescent spot remained visible after this secondary event, at the same position ( $n = 18$ , 14 cells). In some cases the disappearance of these tertiary spots could also be visualized ( $n = 13$ , 9 cells).

There are three possibilities that could give rise to such observations, as shown schematically in Fig. 4: (1) two adjacent vesicles, appearing as one due to our limited spatial resolution, could fuse successively (Fig. 4a); (2) a single vesicle could fuse a few times successively and transiently as in kiss-and-run fusion (Fig. 4b); (3) a

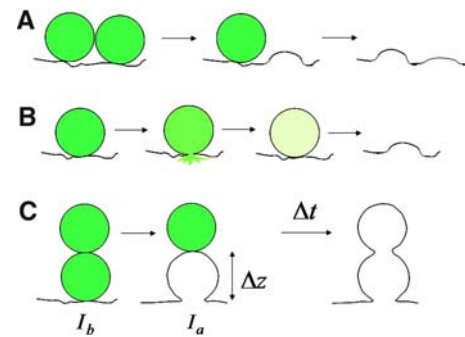


**Fig. 4** Different processes that could generate incomplete or multistep disappearance of a fluorescent spot, as in Fig. 1c. **a** Adjacent vesicles fusing one after the other. **b** Successive and transient fusions of a single vesicle. **c** Sequential fusion.  $I_b$  and  $I_a$  refer to the fluorescence intensity of a spot visualized in TIRFM before and after fusion, respectively. The ratio of these intensities allows calculation of a “virtual jump” distance,  $\Delta z$ , in the  $z$ -direction. The three hypothetical processes shown here would produce distinct  $\Delta z$  statistics, which can be used to evaluate their relative contributions (see text for details).  $\Delta t$  is the delay between two successive fusions occurring at the same spot

sequential fusion event involving two or more vesicles could occur, as depicted in Fig. 4c.

To distinguish between these possibilities, we tracked positions of spots which displayed residual fluorescence in the axial direction ( $z$ -axis) (Materials and methods). These  $z$ -trajectories *do not* refer to any real, physical displacements through space. Rather, they are an abstract, evanescence-depth-dependent measure of fluorescence intensity changes accompanying fusion events displaying residual fluorescence. Thus, we refer to them as “virtual trajectories”. They contain valuable information that can be used to dissect the origin of the residual fluorescence signals, as follows. Each fusion event leaving behind a residual fluorescence signal is associated with a “virtual jump”,  $\Delta z$ , along the  $z$ -axis and away from the membrane, related to the ratio,  $I_a/I_b$ , of the fluorescence intensity of a spot just after to just before an exocytosis:  $\Delta z = -\delta \ln(I_a/I_b)$ . Quite distinct mean values and distributions of these jump sizes are expected for the three possible mechanisms generating them:

1. **Adjacent fusion.** Fusion of one of two adjacent vesicles that cannot be optically resolved would lead, on average, to a drop in the intensity of the spot by a factor of 1/2. That is, for such events  $\Delta z = -\delta \ln(I_a/I_b) = -\delta \ln(1/2)$ , which equals 69 nm and 104 nm for  $\delta = 100$  nm and  $\delta = 150$  nm, respectively.
2. **Transient fusion.** Quite generally, for transient events, the distribution of  $\Delta z$  is expected to be broad and without a characteristic peak, if transient pore opening is a stochastic event with broadly distributed open times. In particular, assuming that the pore open times

are exponentially distributed and that the loss of vesicle contents is determined by the open time of the pore leads to an *exponentially increasing distribution* for  $\Delta z$ , dependent on  $\delta$ , as shown in the Appendix.

3. **Sequential fusion.** For sequential events, fusion of a primary vesicle is accompanied by the loss of a fraction of the total intensity that corresponds approximately to the size of the primary vesicle (Fig. 4c). That is, only in the case of sequential fusion that the “virtual jumps” in the  $z$ -direction accompanying a primary fusion event correspond to a real physical quantity, namely the diameter of the primary vesicle ghost. Hence, the distribution of  $\Delta z$  generated by sequential fusion should nearly match the size distribution of vesicles. Detailed studies of size-distributions of secretory vesicles in enterochromaffin BON cells have not been reported. However, electron micrographs from Parekh et al. (1994), Kim et al. (2001) and our own unpublished data suggest LDCVs in BON cells have sizes similar to those found in bovine chromaffin cells. Detailed studies in bovine chromaffin cells yielded Gaussian, or nearly Gaussian distributions with mean vesicle sizes between 200 and 350 nm, and typical dispersions of  $\sim 10$  to 100 nm (see Parsons et al. 1995; Plattner et al. 1997 and references therein). Thus, sequential exocytosis should lead to a  $\Delta z$  distribution that should be nearly Gaussian, with mean  $\approx 200$ –300 nm. Furthermore, unlike the distributions generated by adjacent or transient fusions, this distribution should be independent of  $\delta$ .

#### Adjacent vesicle fusion

As discussed in the preceding section, virtual jumps in the  $z$ -direction associated with fusion events leaving behind residual fluorescence can be used to identify adjacent fusions. Nonetheless, we decided to use other, independent criteria to identify and separate adjacent events from the other two possible types (transient and sequential events) and rather make use of the virtual  $z$ -jump statistics as an a posteriori test to verify that the remaining events did not contain any significant amount of adjacent fusions.

The first criterion used to detect adjacent fusions is the ellipticity of a fluorescent spot. Two adjacent vesicles, with a diameter of  $\sim 250$  nm each, would appear as an ellipse whose major axis (500 nm) is slightly larger than our optical resolution limit ( $\approx 300$  nm). Fluorescent spots which clearly appeared elliptical were scored as adjacent fusions and eliminated from further analysis. In cases where ellipticity was not obvious, we adjusted the threshold used in the tracking algorithm during tracking of a single spot (dynamic thresholding), such that  $xy$  tracking could be

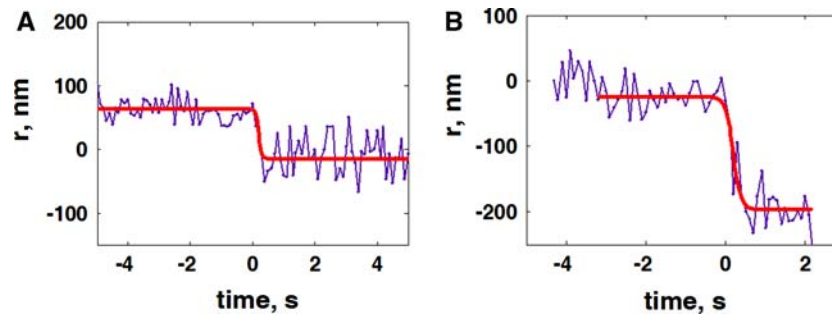
continued with good resolution ( $\lesssim 50$  nm) even after an important sudden drop in the fluorescence intensity (such as following an exocytosis). When one of a pair of two adjacent, 250 nm diameter vesicles (the pair detected as a single spot) disappears, a shift of 125 nm between the centroid of the original spot and the remaining one is expected. Using a somewhat more stringent criterion, we considered events in which the  $xy$  centroid position of the tracked spot shifted  $> r_{sim}100$  nm just after the first exocytosis to be adjacent fusions. Such events were excluded from further analysis.

Figure 5 shows centroid position as a function of time of two fluorescent spots which both disappeared in two sudden, sequential steps. In Fig. 5a, the  $xy$  position of the spot in Fig. 1c is shown as a function of time. The position of the spot shifted by  $\lesssim 80$  nm just following (the first) exocytosis at  $t = 0$ . This exocytosis event was considered not to be due to an adjacent fusion, and included in further analyses aimed at discriminating between sequential and transient events. In Fig. 5b, the centroid position of another spot is shown as a function of time. The position of this spot shifted by  $\sim 170$  nm when an exocytosis occurred at  $t = 0$ . This event was classified as adjacent fusion, and was excluded from further analysis. The virtual jump size,  $\Delta z$ , for this event (recorded using  $\delta = 100$  nm) was equal to 80 nm, which is also consistent with adjacent fusion.

To test how successful we were in detecting and eliminating adjacent fusions, we analyzed the virtual  $z$ -jump statistics on the remaining events displaying residual fluorescence. We saw no systematic differences in the  $\Delta z$ -distributions for data acquired at  $\delta = 100$  nm ( $\langle \Delta z \rangle = 233 \pm 92$  nm,  $n = 75$ , 15 cells) versus  $\delta = 150$  nm ( $\langle \Delta z \rangle = 217 \pm 104$  nm,  $n = 23$ , 7 cells). In comparison, for adjacent fusions one expects, on average,  $\Delta z = 69$  and 104 nm for  $\delta = 100$  nm and  $\delta = 150$  nm, respectively, as explained in the previous section. This suggests that adjacent fusions were indeed successfully detected and excluded from the analyses described in the next section aimed at discriminating between transient and sequential events.

#### Transient versus sequential fusion

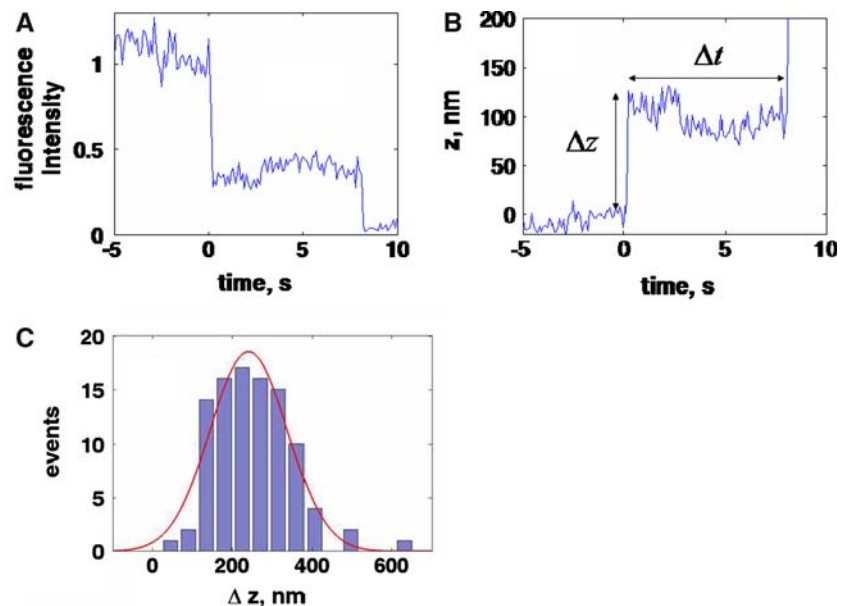
After identification and elimination of adjacent fusion events as described above, remaining fusion events displaying residual fluorescence were analyzed by calculating virtual  $z$ -trajectories and “virtual jumps”,  $\Delta z$ , accompanying fusion events. For transient events, the distribution of  $\Delta z$  is expected to be exponential, whilst for sequential events the distribution of  $\Delta z$  should nearly match the size distribution of vesicles, i.e., a Gaussian (Sect. [Residual fluorescence after an exocytosis, possible mechanisms generating it, and how to distinguish among them using the “virtual trajectory” analysis](#)). Figure 6a, b show the



**Fig. 5** Shift in the  $xy$  centroid position,  $r$ , of a fluorescent spot ( $r = \sqrt{x^2 + y^2}$ ) upon exocytosis. **a** The centroid of the fluorescent spot depicted in Fig. 1c shifted by an amount  $\Delta r_{\text{exo}} < 100$  nm as exocytosis occurred at  $t = 0$ . This event was not classified as adjacent fusion and was included in subsequent analyses aimed at distinguishing between transient and sequential events. **b** Centroid position of another fluorescent spot. In this case, the position of the tracked spot shifted  $\Delta r_{\text{exo}} > 100$  nm as exocytosis occurred. This event was classified as adjacent fusion and was not included in further analysis.

Thick lines are fits to data of the form  $r(t) = a + \Delta r / (1 + \exp((t-t_s)/\tau))$ , where  $a$  measures the value of  $r$  after exocytosis ( $t > 0$ ),  $t_s$  accounts for a possible offset in the position of the fitted vertical shift with respect to  $t = 0$  (selected manually from intensity vs. time traces),  $\tau$  measures the speed at which the shift in  $r$  occurs and  $\Delta r$  is the amount of shift in nm. The fit in **a** yielded  $a = -15$  nm,  $\Delta r = 78$  nm,  $\tau = 0.05$  s, and  $t_s = 0.20$  s, while the fit in **b** resulted in  $a = -196$  nm,  $\Delta r = 172$  nm,  $\tau = 0.10$  s, and  $t_s = 0.20$  s

**Fig. 6** Calculation of virtual jump sizes in the  $z$ -trajectories. **a** Fluorescence intensity as a function of time for the spot in Fig. 1c. **b** Positions calculated from the intensity trace in **a** (see “Materials and methods”). **c** Distribution of virtual jump sizes,  $\Delta z$  ( $n = 98$ , 22 cells). The Gaussian fit shown yielded  $\langle \Delta z \rangle = 241 \pm 69$  nm



fluorescence intensity as a function of time for the spot in Fig. 1c and the  $z$ -position calculated from the intensity trace, respectively. The distribution of values calculated from 98 similar events is shown in Fig. 6c. A Gaussian fit yielded  $\langle \Delta z \rangle = 241 \pm 69$  nm ( $R^2 = 0.94$ ), matching quite well LDCV sizes of 200–300 nm deduced from electron micrographs of BON cells (Parekh et al. 1994; Kim et al. 2001; and our own unpublished results). In addition, essentially the same distribution was obtained using  $\delta = 100$  and 150 nm. These observations suggest that most of the multi-exocytotic events originate from sequential fusions involving two or more vesicles and not from successive transient fusions of the same vesicle.

The frequency of events leaving behind residual fluorescence detected at two different evanescence depths independently supports the above-mentioned conclusion. Transient fusion should be detected with the same efficiency regardless of the value of the evanescent depth,  $\delta$ . On the other hand, a smaller proportion of sequential events should be detected when thinner depths are probed, since it would be more difficult to detect deep-lying vesicles. Using a small range of  $\delta$  values in preliminary studies, we detected residual fluorescence after an exocytosis (with or without a second or third exocytosis at the same spot) in 9.4% (112/1,196) and 19.2% (101/525) of all exocytic events at  $\delta = 100$  nm (31 cells) and  $\delta = 150$  nm (24 cells),

respectively, suggesting that sequential events should be at the origin of an important portion of such observations (Table 1).

#### Kinetics of primary versus higher order fusion events

An important question concerns the fusion readiness of vesicles lying in deeper layers compared to vesicles at the cell membrane. To answer this question, we compared fusion kinetics of primary vesicles (lying closest to the cell membrane, regardless of whether they were targets of secondary events later) to those of higher order vesicles (involved in secondary, tertiary, etc. events). Figure 7a shows the number of primary exocytosis events as a function of time for BON cells stimulated by digitonin permeabilization in the presence of 30  $\mu\text{M}$  free calcium (317 events, 40 cells). In these experiments, intracellular calcium,  $[\text{Ca}^{2+}]_i$ , should rise rapidly and be clamped to 30  $\mu\text{M}$  following permeabilization. Since there was variability in the speed of permeabilization from cell to cell, kinetic curves from different cells are shifted horizontally such that  $t = 0$  corresponds to the first exocytosis event observed in a cell (indicating that the cell was successfully permeabilized). A fit to the first 60 s of data in the form  $n(t) = N_\infty [1 - \exp(-t/\tau)]$  resulted in  $N_\infty = 292$  and  $\tau = 10.2 \pm 0.2$  s ( $R^2 = 0.99$ ). Only the first 60 s were used in the analysis, since escape of cytosolic factors through digitonin induced pores in the cell membrane may affect kinetics at longer times (Sarafian et al. 1987; S. Tran, unpublished results). In comparison, time lags between pairs of successive events are shown in Fig. 7b ( $n = 27$ , 10 cells). Since tertiary events were rarely detected, these lags are mainly between primary and secondary events. A fit of the same form as used in Fig. 7a yielded  $N_\infty = 28$  and  $\tau = 9.0 \pm 1.2$  s ( $R^2 = 0.98$ ). Thus, there is no significant difference between the kinetics of primary and higher order fusion events.

In experiments wherein UV uncaging of calcium was used to increase  $[\text{Ca}^{2+}]_i$  and stimulate exocytosis,  $[\text{Ca}^{2+}]_i$

was not clamped to a fixed value but rather varied in a less well-controlled manner. Thus we do not use these measurements for making a quantitative comparison between kinetics of primary and higher order fusions.

#### Discussion

Understanding factors controlling secretion from neuroendocrine carcinoid tumors is important for developing treatments. The human neuroendocrine carcinoid BON cell line is one of the only cell lines successfully mimicking morphological and physiological characteristics of such tumors and have been widely used as a model to study secretion of gut peptides (Evers et al. 1994; Li et al. 2005a, 2004; Jackson et al. 2006; Mergler 2003; Mergler et al. 2005). We had previously characterized secretion in BON cell populations (Tran et al. 2004) and studied dynamics of single secretory vesicles in BON cells under resting conditions (Huet et al. 2006). Here we have used digitonin permeabilization in the presence of calcium buffered at 30  $\mu\text{M}$  or ‘uncaging’ of calcium from a photolabile chelator loaded into cells to trigger exocytosis.

Three main types of single exocytotic events were observed: simple fusions (Fig. 1a), orphan events (Fig. 1b) and events with incomplete disappearance of a fluorescent spot (Fig. 1c). Similar observations had been reported by others in previous TIRFM studies (Ma et al. 2004, Taraska et al. 2003, Allersma et al. 2004, 2006). However, there was much ambiguity about the mechanisms responsible for generating the two latter types of event. Here, thanks to a combination of two-color imaging, variable angle TIRFM, and novel statistical analyses, we have shown that residual fluorescence following an exocytosis event and orphan fusions (occurring within cellular footprints) are part of the same basic mechanism, namely shape retention of fused primary vesicle ghosts which become targets for sequential fusions with deeper lying vesicles. For a vesicle pair

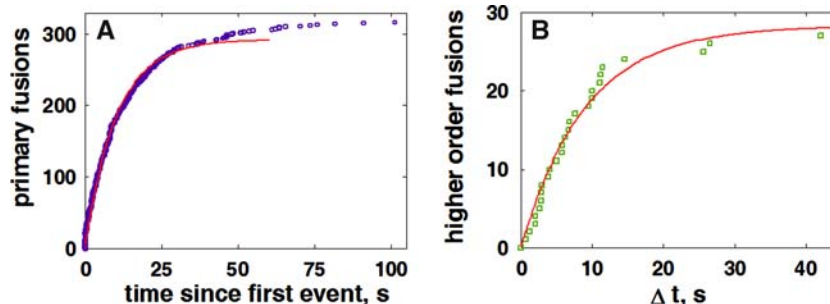


**Fig. 7** Fusion kinetics for primary and higher order events for permeabilization experiments in which  $[\text{Ca}^{2+}]_i = 30$   $\mu\text{M}$ . **a** Number of primary fusion events detected as a function of time ( $n = 317$ , 40 cells). Time  $t = 0$  corresponds to the first fusion event detected in each cell, indicating successful permeabilization. Exponential fit (red

line) yielded  $\tau = 10.2 \pm 0.2$  s ( $R^2 = 0.99$ ). **b** Distribution of lag times between pairs of successive fusions at a given spot for the same experiments ( $n = 27$ , 10 cells). Exponential fit (red line) yielded  $\tau = 9.0 \pm 1.2$  s ( $R^2 = 0.98$ )

undergoing sequential fusion observed using TIRFM, there are two possibilities, as depicted schematically in Fig. 8:

1. The local S/N is good enough to allow detection of the secondary vesicle, queued up behind the primary one, following exocytosis of the primary vesicle. This would generate partial disappearance of the original fluorescent spot.
2. The local S/N does not allow detection of the secondary vesicle which is located 200–300 nm away from the cell membrane. However, upon fusion of this secondary vesicle with the primary ghost, its fluorophores would be released into the conduit leading to the extracellular space. While crossing the conduit to reach the space between the adherent cell and the coverslip, the labels enter the evanescent field and become visible shortly before diffusing away. This would generate an orphan fusion event.

We have shown that, overall, a significant portion of exocytosis (~25%, see below) occurs via sequential fusion and that deeper lying vesicles are as fusion-ready as primary vesicles located very near the cell membrane. In this system, transient, kiss-and-run type of fusion events, if they exist, are only a minor contributor that we cannot detect.

Another major achievement of this work is that, to the best of our knowledge, it is the first quantitative report on sequential fusion using TIRFM, despite the long running and widespread use of this technique in studies of secretory mechanisms.

#### Extent of sequential fusion

If both orphans and residual fluorescence are part of the same basic mechanism as we have argued above, we may

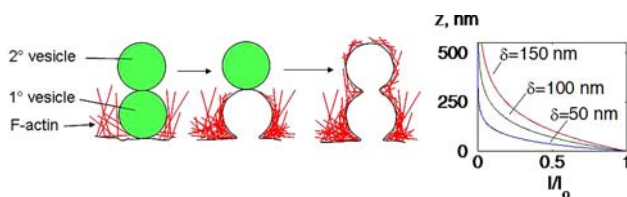


**Fig. 8** Schematic description of sequential fusion. The theoretical evanescent excitation field profile is drawn on the right, for different evanescence depths,  $\delta$ , as marked. After exocytosis of the primary vesicle, the secondary one would be detected as a residual fluorescent signal only if the local S/N is favorable. The secondary vesicle may fuse at a later time if the observation time is sufficiently long. If the local S/N is poor, on the other hand, the secondary vesicle would only become manifest indirectly as an orphan fusion event upon its fusion with the ghost of the primary vesicle. For sequential fusion to occur to a significant extent, shapes of vesicles which undergo fusion must be conserved for a time comparable to the mean lag between successive sequential events, i.e. about 10 s here. Shape conservation is likely to be by rapid F-actin coating of freshly fused vesicle ghosts

expect their overall proportion to remain roughly constant as the evanescence depth,  $\delta$ , is varied, since detection of orphans decreases with increasing  $\delta$  while that of residual fluorescence increases. Remarkably, the total fraction of orphan events and events resulting in residual fluorescence is nearly the same for data acquired at  $\delta = 100$  and 150 nm, as shown in Table 1. Thus we suggest that 23–26% of all exocytotic events in the basal membranes of BON cells occur through sequential fusion.

How accurate is this estimate? There are at least three sources of under-counting of sequential events: (1) our acquisition rate is likely to be too slow to detect all orphan events, since with 10 Hz acquisition, an orphan event typically lasts only 1–2 frames, (2) we probably classified too many fusions leaving behind residual fluorescence as adjacent fusions. Some of these events could in fact be sequential fusions with the secondary vesicle located off the  $z$ -axis passing through the center of the primary vesicle ghost, and (3) use of transient expression of the vesicular contents marker, NPY-GFP, may leave some vesicles unlabeled (LDCV turnover is slow and takes days) and thus lead to an underestimate of sequential fusion (e.g., if some of the secondary, tertiary vesicles are unlabeled their contribution to sequential events would not be counted). On the other hand, not all residual fluorescent signals were observed to disappear. Even if longer observation times are used, it is possible that only a fraction of the secondary vesicles would undergo fusion, similar to primary vesicles of which only a fraction fuse even under extended stimulation. These effects leading to under- and over-counting should compensate each other, at least to some degree.

#### Alternative mechanisms that could generate orphan fusions

Two alternative explanations have been put forward by Allersma et al. (2004, 2006) for explaining orphan events observed in TIRFM studies of bovine chromaffin cells whose LDCV membranes were labeled using the v-SNARE VAMP-GFP: (1) membrane folds (generated by a mechanism other than recently fused vesicle ghosts) keep vesicles behind the fold outside the evanescent field and thus render them invisible, and (2) there exists a particular population of rapidly moving vesicles which cross the entire evanescent field, dock and fuse, all within a single imaging plane or faster (i.e., in less than ~100 ms). We refer to these latter as “ballistic” vesicles.

Typical separations between adherent cells and their substrates are between 20 and 80 nm (Curtis 1964; Lanni et al. 1985; Olveczky et al. 1997; S. Huet, unpublished observations). These values are small compared to the evanescence depths used here (100 and 150 nm), but not very far from  $\delta = 55$  nm used by Allersma et al. (2004,

2006). Thus, mechanism (1) above seems unlikely to be responsible for generating orphan events in our system, although it is a likely contributor to the observations of Allersma et al. (2004, 2006). Alternatively, if ballistic vesicles generate most of the orphan events, at most ~50% more orphan events should be detected at  $\delta_1 = 100$  nm compared to  $\delta_2 = 150$  nm, as shown in Appendix. Contrary to this expectation, Table 1 indicates almost 100% more orphan events at  $\delta = 100$  nm compared to  $\delta = 150$  nm. Furthermore, an analysis of the distribution of times spent at the cell membrane prior to exocytosis by vesicles arriving to the cell membrane from at least 100 nm away indicates a smooth and continuously decreasing function that can be well-described by an exponential with a decay time of  $\tau_{\text{newcomer}} \sim 10$  s (E. Karatekin et al., in preparation). Among such “newcomer” vesicles, those with the shortest residency times ( $\lesssim 0.1$  s, our typical acquisition interval) at the cell membrane could indeed be classified as “ballistic” events, even though these vesicles do not necessarily belong to a distinct class. Their frequency compared to the rest of newcomers is  $t_{\text{ballistic}}/\tau_{\text{newcomer}} \approx 0.1 \text{ s} / 10 \text{ s} = 1\%$ . Since newcomers make up only 30–40% of all fused vesicles (E. Karatekin et al., in preparation), ballistic events would contribute only 0.3–0.4% to the orphans observed here compared to all fusion events. Finally, ballistic vesicles must have axial speeds of at least a few micrometers per second in order to cross the entire evanescent field in less than 0.1 s, which is much faster than what may be expected for vesicles moving along microtubules (Manneville et al. 2003; Huet et al. 2006). Thus, ballistic vesicles are unlikely to contribute to orphan fusions we have observed. Rather, our data is consistent with most orphan events (occurring well within cellular footprints) being generated by a sequential fusion mechanism.

#### TIRFM versus two-photon imaging to study sequential fusion

Sequential exocytosis was previously described using two-photon, and confocal microscopy approaches. In these experiments, typically a tissue section is bathed in a solution with a soluble extracellular label which diffuses into the thin inter-cellular space, rendering cellular outlines visible. When exocytosis occurs and the shape of the vesicular ghost survives long enough to be detected, the soluble label fills the vesicular ghost and renders it visible (i.e. a small fluorescent spot appears suddenly). Several possible outcomes follow thereafter: the ghost may collapse into the cell membrane (the spot disappears), may linger much longer than the typical collapse time (probably indicating resealing of a transient fusion pore), or a second fluorescent spot may pop up behind the first one (indicating sequential fusion). Two-photon microscopy seems to be an

ideal tool for such studies, since it can penetrate deep into tissues, provides high spatial resolution with small excitation volumes (leading to low photobleaching), and the labeling strategy allows unambiguous detection of single sequential fusion events.

Two-photon microscopes present some disadvantages; however, they are not readily available, costly, and difficult to use in other studies related to secretion, such as 3D tracking of single secretory vesicles. In addition, acquisition rates are typically limited to ~1 Hz (higher rates are possible but at the expense of the size of the scanned region). On the other hand, commercial TIRF microscopes are readily available and many tools for studying dynamics of single vesicles and their exocytosis have been developed in many laboratories. Furthermore, faster acquisition rates are readily achieved compared to two-photon imaging (e.g., up to 40 Hz was used here). For these reasons, TIRFM has arguably been the single most successful tool for secretion studies (An and Zenisek 2004; Steyer and Almers 2001; Axelrod 2003; Schneckenburger 2005). Nevertheless, to the best of our knowledge, sequential exocytosis had never been unequivocally detected using TIRFM before this report. This is paradoxical, given the huge body of work on exocytosis carried out using TIRFM and the widespread occurrence of sequential exocytosis in many different cell types as demonstrated by two-photon and confocal microscopy approaches (Nemoto et al. 2001; Kishimoto et al. 2005, 2006; Pickett and Edwardson 2006). The only previous TIRFM study that we are aware of in which sequential fusion was suggested to play a role is by Allersma et al. (2004) who stimulated bovine chromaffin cells using the nicotinic agonist 1,1 dimethyl-4-phenylpiperzinium (DMPP). They noted that “approximately 10% of the exocytotic sites were much more likely to occur within a granule diameter of a previous event than can be accounted for by chance, suggestive of sequential (piggy-back) exocytosis that has been observed in other cells.” The authors did not report the nature of the events (with residual fluorescence or orphan fusions) occurring in these “hot spots” making it difficult to judge if sequential exocytosis was indeed likely to have occurred.

Why has it been so difficult to detect sequential exocytosis using TIRFM? A first difficulty arises from the typical labeling strategy employed in TIRFM in which contents of vesicles are marked. The label disappears upon fusion of the vesicle with the cell membrane; thus vesicle ghosts lingering at the cell membrane are invisible, unless special labeling strategies are employed as in Taraska et al. (2003) and Allersma et al. (2004), or here. Another difficulty has been the limitation of the observation zone to a very thin layer (50–200 nm) in TIRFM. This makes it difficult to detect deeper lying, unfused, labeled vesicles after a primary fusion event. The problem is aggravated

when the smallest evanescence depths are used, as typical of commercial, through-the-lens setups. Thinner depths are desirable to get better S/N, but residual fluorescence from secondary vesicles queuing behind a ghost would be more difficult to detect. Finally, a much more serious difficulty has been the quantitative interpretation of fusion events which leave behind residual fluorescence signals and orphan events. In the past, fusion events leaving behind residual fluorescence in TIRFM studies of chromaffin and PC-12 cells have been assumed to be due to transient, kiss-and-run type of fusions (Taraska et al. 2003; Ma et al. 2004). Orphan fusions, on the other hand, have been interpreted to be due to ballistic vesicles, in chromaffin cells (Allersma et al. 2006, 2005). Although some of these interpretations are likely to be correct, the possibility of sequential fusion for explaining such events had not been examined previously. It is likely that sequential fusion contributed, at least partially, to these observations, given the frequent occurrence of sequential fusion in both of these cell types as detected by two-photon imaging (Kishimoto et al. 2006, 2005). Here, we have shown how to overcome these difficulties thanks to a combination of variable-angle TIRFM, two-color imaging, and novel statistical analyses. Our overall findings are consistent with residual fluorescence following a fusion event and orphan fusions being generated by the same basic mechanism, namely sequential exocytosis.

### Mechanistic implications

Mechanistically, frequent occurrence of sequential fusion requires a major revision of our current thinking about the fusion-readiness and translocation of secretory vesicles lying deep (>200–300 nm) inside the cytosol toward the cell-membrane. For example, the precise role of the 300–500 nm thick dense actin cortex in secretion is a subject of intense debate. Some workers proposed that it may constitute a barrier to exocytosis by hindering vesicles from reaching the cell membrane (Trifaró and Vitale 1993; Trifaró et al. 2000), while others suggested that the cortex plays an active role in delivering vesicles to fusion sites at the cell membrane (Lang et al. 2000; Oheim and Stuhmer 2000). Deep-lying vesicles undergoing sequential fusion do not need to move across the dense actin cortex to undergo exocytosis, as previously noted by Kishimoto et al. (2006).

As for the fusion-readiness of deep-lying vesicles, the mean lag between successive fusions,  $\Delta t$ , is comparable to the mean time required for the fusion of primary vesicles (Fig. 7). This suggests that deep-lying vesicles are just as fusion-ready as vesicles already at the cell membrane before stimulation, as proposed earlier (Kishimoto et al. 2006).

Although the ultimate fate of fused vesicle ghosts was outside the scope of this study, it is reasonable to expect that they may be endocytosed en bloc, avoiding time- and energy-consuming lipid and protein sorting that would be required upon full collapse into, and mixing with, the plasma membrane (Sokac and Bement 2006; Taraska et al. 2003). Overall, then, sequential exocytosis may allow a cell to respond robustly and with minimal effort to strong stimulation.

An interesting observation reported by Kishimoto et al. (2006) in adrenal slices is that shape retention after fusion (and hence sequential fusions) were more common in cellular regions facing neighboring cells as compared to regions directly facing the bath solution. This suggests that cell-cell and/or cell-substrate adhesion may regulate retention of vesicular ghost shapes after exocytosis and sequential fusion. Hence, tuning cell-substrate interactions in a controlled manner, e.g., by micro-contact printing of extracellular matrix patterns onto substrates (Théry et al. 2005), could lead to a better understanding of the mechanisms governing “kiss-and-coat” and sequential fusions. Equipped with the novel analysis methods presented here, TIRFM is perfectly suited for such studies.

**Acknowledgements** We thank Ben O’Shaughnessy, Françoise Brochard-Wyart, Axel Buguin and Bruno Gasnier for carefully reading the manuscript, and Pablo A. Caviades and members of the UPR 1929 for fruitful discussions. This work was supported by the CNRS and the U. Paris 7 Denis Diderot. S. Huet was supported by the Direction Générale de l’Armement and the Association pour la Recherche sur le Cancer.

### Appendix

#### Distribution of $\Delta z$ for transient fusions

The probability density function of the fraction of vesicle contents released was calculated by Jones and Friel (2006), assuming (1) fusion pore lifetimes are exponentially distributed ( $\tau_p$ ), as expected for simple channel openings, and (2) vesicle contents are lost through the fusion pore with an exponential time course ( $\tau_D$ ):

$$dP/dF = A(1 - F)^{A-1}, \quad (1)$$

where  $A \equiv \tau_D/\tau_p$ , and  $F$  is the fraction of vesicle contents released in a transient pore opening. For our experiments,  $F = 1 - r$ , where  $r = I_a/I_b$  is the ratio of the fluorescence intensity of a spot just after ( $I_a$ ) to just before ( $I_b$ ) a fusion. Thus, (1) can be written as

$$y = Ar^{A-1}, \quad (2)$$

where  $y = dP/dF$ . We wish to calculate the distribution of “virtual jump” sizes,  $\Delta z = -\delta \ln r$ , in the  $z$ -space (see

“Materials and methods”). This is obtained trivially by substituting  $r = e^{-\Delta z/\delta}$  into (2):

$$y = Ae^{-(A-1)\Delta z/\delta}. \quad (3)$$

In our experiments, the great majority of fluorescent spots disappeared in a single fusion ( $F = 1$ ), implying  $A \equiv \tau_D/\tau_P < 1$ . That is, the factor  $-(A-1)$  in (3) is  $>0$ , and  $y$  increases exponentially as a function of  $\Delta z$  without bound. The experimentally measured distribution of  $\Delta z$ , shown in Fig. 6c, is clearly not exponential, implying that transient fusions do not contribute to our observations in any significant way.

#### Frequency of orphan events generated by “ballistic” vesicles

Orphan events generated by ballistic vesicles should be observed more often when thinner evanescence depths,  $\delta$ , are used. For such vesicles, there are two extreme cases, depending on the time to cross the evanescent field ( $\tau_{\text{cross}}$ ) and the time spent at the membrane before fusion ( $\tau_{\text{mb}}$ ). A vesicle would be visible for a duration that is the total of these two timescales, i.e.  $\tau_{\text{vis}} = \tau_{\text{cross}} + \tau_{\text{mb}}$ . The crossing time depends on the evanescence depth,  $\delta$ , becoming longer with larger  $\delta$  ( $\tau_{\text{cross}} \propto \delta/v$ , where  $v$  is the average speed with which a vesicle moves toward the membrane), whereas  $\tau_{\text{mb}}$  is independent of it. In the limit  $\tau_{\text{cross}} \gg \tau_{\text{mb}}$ , we expect that the fraction of detected orphan events,  $f_{\text{orphan}}$ , scales inversely with  $\tau_{\text{cross}}$ , i.e.  $f_{\text{orphan}} \sim \delta^{-1}$ . Thus, comparing data acquired at  $\delta_1 = 100$  nm and  $\delta_2 = 150$  nm, we expect  $f_{\text{orphan}}(\delta_1)/f_{\text{orphan}}(\delta_2) = \delta_2/\delta_1 = 150 \text{ nm}/100 \text{ nm} = 1.5$ , that is  $\sim 50\%$  more orphan events should be detected at  $\delta_1 = 100$  nm compared to  $\delta_2 = 150$  nm. In the other extreme, i.e.  $\tau_{\text{cross}} \ll \tau_{\text{mb}}$ , orphan events should be detected with the same efficiency regardless of the value of  $\delta$  since ballistic vesicles should spend most of their short stays in the evanescent field at the cell membrane. Overall, at most 50% more ballistic orphans should be detected at  $\delta = 100$  nm compared to  $\delta = 150$  nm.

#### References

Allersma MW, Wang L, Axelrod D, Holz RW (2004) Visualization of regulated exocytosis with a granule-membrane probe using total internal reflection microscopy. *Mol Biol Cell* 15:4658–4668

Allersma MW, Bittner MA, Axelrod D, Holz RW (2006) Motion matters: secretory granule motion adjacent to the plasma membrane and exocytosis. *Mol Biol Cell* 17:2424–2438

An S, Zenisek D (2004) Regulation of exocytosis in neurons and neuroendocrine cells. *Curr Opin Neurobiol* 14:522–530

Aravanis AM, Pyle JL, Tsien RW (2003) Single synaptic vesicles fusing transiently and successively without loss of identity. *Nature* 423:643–647

Axelrod D (2003) Total internal reflection fluorescence microscopy in cell biology. *Methods Enzymol* 361:1–33

Cheezum MK, Walker WF, Guilford WH (2001) Quantitative comparison of algorithms for tracking single fluorescent particles. *Biophys J* 81:2378–2388

Curtis AS (1964) The mechanism of adhesion of cells to glass. a study by interference reflection microscopy. *J Cell Biol* 20:199–215

Evers BM, Townsend J, C M, Upp JR, Allen E, Hurlbut SC, Kim SW, Rajaraman S, Singh P, Reubi JC, Thompson JC (1991) Establishment and characterization of a human carcinoid in nude mice and effect of various agents on tumor growth. *Gastroenterology* 101:303–311

Evers BM, Ishizuka J, Townsend J, C M, Thompson JC (1994) The human carcinoid cell line, BON. A model system for the study of carcinoid tumors. *Ann N Y Acad Sci* 733:393–406

Fohr KJ, Warchol W, Gratz M (1993) Calculation and control of free divalent cations in solutions used for membrane fusion studies. *Methods Enzymol* 221:149–157

Huet S, Karatekin E, Tran VS, Fanget I, Cribier S, Henry JP (2006) Analysis of transient behavior in complex trajectories: application to secretory vesicle dynamics. *Biophys J* 91:3542–3559

Jackson LN, Li J, Chen LA, Townsend CM, Evers BM (2006) Overexpression of wild-type PKD2 leads to increased proliferation and invasion of BON endocrine cells. *Biochem Biophys Res Commun* 348:945–949

Jones SW, Friel DD (2006) The amplitude distribution of release events through a fusion pore. *Biophys J* 90:L39–L41

Kim M, Javed NH, Yu JG, Christofi F, Cooke HJ (2001) Mechanical stimulation activates G $\alpha_q$  signaling pathways and 5-hydroxytryptamine release from human carcinoid BON cells. *J Clin Invest* 108:1051–1059

Kishimoto T, Liu TT, Hatakeyama H, Nemoto T, Takahashi N, Kasai H (2005) Sequential compound exocytosis of large dense-core vesicles in PC12 cells studied with TEPIQ (two-photon extracellular polar-tracer imaging-based quantification) analysis. *J Physiol* 568:905–915

Kishimoto T, Kimura R, Liu TT, Nemoto T, Takahashi N, Kasai H (2006) Vacuolar sequential exocytosis of large dense-core vesicles in adrenal medulla. *Embo J* 25:673–682

Lang T, Wacker I, Steyer J, Kaether C, Wunderlich I, Soldati T, Gerdes H-H, Almers W (1997) Ca $^{++}$ -triggered peptide secretion neurotechnique in single cells imaged with Green Fluorescent Protein and evanescent-wave microscopy. *Neuron* 18:857–863

Lang T, Wacker I, Wunderlich I, Rohrbach A, Giese G, Soldati T, Almers W (2000) Role of actin cortex in the subplasmalemmal transport of secretory granules in PC-12 cells. *Biophys J* 78:2863–2877

Lanni F, Waggoner AS, Taylor DL (1985) Structural organization of interphase 3T3 fibroblasts studied by total internal reflection fluorescence microscopy. *J Cell Biol* 100:1091–1102

Li J, O’Connor KL, Hellmich MR, Greeley GH Jr, Townsend CM Jr, Evers BM (2004) The role of protein kinase D in neurotensin secretion mediated by protein kinase C- $\alpha/\delta$  and Rho/Rho kinase. *J Biol Chem* 279:28466–28474

Li J, O’Connor KL, Greeley GH Jr, Blackshear PJ, Townsend CM Jr, Evers BM (2005a) Myristoylated alanine-rich C kinase substrate-mediated neurotensin release via protein kinase C- $\delta$  downstream of the Rho/ROK pathway. *J Biol Chem* 280:8351–8357

Li N, Wang Q, Li J, Wang X, Hellmich MR, Rajaraman S, Greeley GH Jr, Townsend CM Jr, Evers BM (2005b) Inhibition of mitochondrial gene transcription suppresses neurotensin secretion in the human carcinoid cell line BON. *Am J Physiol Gastrointest Liver Physiol* 288:G213–G220

Lindau M, Alvarez de Toledo G (2003) The fusion pore. *Biochim Biophys Acta* 1641:167–173

- Ma L, Bindokas VP, Kuznetsov A, Rhodes C, Hays L, Edwardson JM, Ueda K, Steiner DF, Philipson LH (2004) Direct imaging shows that insulin granule exocytosis occurs by complete vesicle fusion. *Proc Natl Acad Sci USA* 101(25):9266–9271
- Manneville JB, Etienne-Manneville S, Skehel P, Carter T, Ogden D, Ferenci M (2003) Interaction of the actin cytoskeleton with microtubules regulates secretory organelle movement near the plasma membrane in human endothelial cells. *J Cell Sci* 116:3927–3938
- Mergler S (2003)  $Ca^{2+}$  channel characteristics in neuroendocrine tumor cell cultures analyzed by color contour plots. *J Neurosci Methods* 129:169–181
- Mergler S, Wiedenmann B, Prada J (2003) R-type  $Ca^{2+}$ -channel activity is associated with chromogranin A secretion in human neuroendocrine tumor BON cells. *J Membr Biol* 194:177–186
- Mergler S, Strauss O, Strowski M, Prada J, Drost A, Langrehr J, Neuhaus P, Wiedenmann B, Ploekinger U (2005) Insulin-like growth factor-1 increases intracellular calcium concentration in human primary neuroendocrine pancreatic tumor cells and a pancreatic neuroendocrine tumor cell line (BON-1) via R-type  $Ca^{2+}$  channels and regulates chromogranin a secretion in BON-1 cells. *Neuroendocrinology* 82:87–102
- Nemoto T, Kimura R, Ito K, Tachikawa A, Miyashita Y, Iino M, Kasai H (2001) Sequential-replenishment mechanism of exocytosis in pancreatic acini. *Nat Cell Biol* 3:253–258
- Nemoto T, Kojima T, Oshima A, Bito H, Kasai H (2004) Stabilization of exocytosis by dynamic F-actin coating of zymogen granules in pancreatic acini. *J Biol Chem* 279:37544–37550
- Oheim M, Stühmer W (2000) Tracking chromaffin granules on their way through the actin cortex. *Eur Biophys J* 29:67–89
- Olveczky BP, Periasamy N, Verkman AS (1997) Mapping fluorophore distributions in three dimensions by quantitative multiple angle-total internal reflection fluorescence microscopy. *Biophys J* 73:2836–2847
- Parekh D, Ishizuka J, Townsend CM Jr, Haber B, Beauchamp RD, Karp G, Kim SW, Rajaraman S, Greeley G Jr, Thompson JC (1994) Characterization of a human pancreatic carcinoid in vitro: morphology, amine and peptide storage, and secretion. *Pancreas* 9:83–90
- Parsons TD, Coorssen JR, Horstmann H, Almers W (1995) Docked granules, the exocytic burst, and the need for ATP hydrolysis in endocrine cells. *Neuron* 15:1085–1096
- Patton C, Thompson S, Epel D (2004) Some precautions in using chelators to buffer metals in biological solutions. *Cell Calcium* 35:427–431
- Pickett JA, Edwardson JM (2006) Compound exocytosis: mechanisms and functional significance. *Traffic* 7:109–116
- Plattner H, Artalejo AR, Neher E (1997) Ultrastructural organization of bovine chromaffin cell cortex-analysis by cryofixation and morphometry of aspects pertinent to exocytosis. *J Cell Biol* 139:1709–1717
- Sarafian T, Aunis D, Bader MF (1987) Loss of proteins from digitonin-permeabilized adrenal chromaffin cells essential for exocytosis. *J Biol Chem* 262:16671–16676
- Schneckenburger H (2005) Total internal reflection fluorescence microscopy: technical innovations and novel applications. *Curr Opin Biotechnol* 16:13–18
- Shin W, Gillis KD (2006) Measurement of changes in membrane surface morphology associated with exocytosis using scanning ion conductance microscopy. *Biophys J* 91:L63–L65
- Sokac AM, Bement WM (2006) Kiss-and-coat and compartment mixing: coupling exocytosis to signal generation and local actin assembly. *Mol Biol Cell* 17:1495–1502
- Steyer JA, Almers W (2001) A real-time view of life within 100 nm of the plasma membrane. *Nat Rev Mol Cell Bio* 2:268–275
- Steyer JA, Horstmann H, Almers W (1997) Transport, docking and exocytosis of single secretory granules in live chromaffin cells. *Nature* 388:474–478
- Takahashi N, Kishimoto T, Nemoto T, Kadowaki T, Kasai H (2002) Fusion pore dynamics and insulin granule exocytosis in the pancreatic islet. *Science* 297:1349–1352
- Taraska JW, Perrais D, Ohara-Imaizumi M, Nagamatsu S, Almers W (2003) Secretory granules are recaptured largely intact after stimulated exocytosis in cultured endocrine cells. *Proc Natl Acad Sci USA* 100:2070–2075
- Théry M, Racine V, Pépin A, Piel M, Chen Y, Sibarita J, Bornens M (2005) The extracellular matrix guides the orientation of the cell division axis. *Nature Cell Biol* 7:947–953
- Tran VS, Marion-Audibert AM, Karatekin E, Huet S, Cribier S, Guillaumie K, Chapuis C, Desnos C, Darchen F, Henry JP (2004) Serotonin secretion by human carcinoid BON cells. *Ann N Y Acad Sci* 1014:179–188
- Trifaró J-M, Vitale ML (1993) Cytoskeleton dynamics during neurotransmitter release. *Trends Neurosci* 16:466–472
- Trifaró J-M, Rosé SD, Lejen MT, Elzagallaai A (2000) Two pathways control chromaffin cell cortical F-actin dynamics during exocytosis. *Biochimie* 82:339–352